COMPDYN 2009
ECCOMAS Thematic Conference on
Computational Methods in Structural Dynamics and Earthquake Engineering
M. Papadrakakis, N.D. Lagaros, M. Fragiadakis (eds.)
Rhodes, Greece, 22-24 June 2009

# STRENGTH REDUCTION FACTORS FOR THE DYNAMIC INSTABILITY OF OSCILLATORS WITH NON-TRIVIAL BACKBONES

**Dimitrios Vamvatsikos[1], Sinan D. Akkar[2], and Eduardo Miranda[3]**

[1]University of Cyprus
Nicosia 1678, Cyprus
e-mail: divamva@ucy.ac.cy

[2] Middle East Technical University
Ankara, Turkey
e-mail: sakkar@metu.edu.tr

[3] Stanford University
Stanford, CA 94305-4020, USA
e-mail: emiranda@stanford.edu

**Keywords:** Oscillator, Hysteretic Systems, Nonlinear Dynamic Analysis, Dynamic Instability, Seismic Performance.

**Abstract.** *Novel empirical relationships are introduced to estimate the median, mean and dispersion of strength ratios to cause dynamic instability in oscillators with non-trivial backbones and arbitrary periods. The backbones investigated range from a simple bilinear elastic-negative shape to a trilinear that includes an elastic, a hardening and a negative stiffness segment that terminates at zero strength. Using 72 ground motion records that were recorded on firm soil we calculate the mean, median, 16% and 84% percentiles of the corresponding lateral strength ratios required for the appearance of dynamic instability. Processing of the results shows the influence of the oscillator parameters to the occurrence of dynamic instability: Lengthening the oscillator period, delaying the onset of negative stiffness and decreasing the negative slope are all shown to delay the appearance of collapse. On the other hand, contrary to current engineering intuition, increasing the hardening stiffness while maintaining the same period and coincident negative branches has only a small effect on the onset of instability. Using nonlinear regression, parametric equations are developed that can accurately capture such effects in a simple, easy-to-use formula.*

## 1 INTRODUCTION

The estimation of the collapse capacity of structures under seismic excitation has stimulated the interest of the earthquake engineering community since its early days. Driven by the abundant evidence of structural collapses in historic earthquakes this search has been going on for years. Of particular interest is the dynamic instability of structures under seismic loads, caused by the reduction in lateral strength due to the formation of a mechanism of hinges, the influence of P-$\Delta$ or both. Several researchers have recognized the need to understand and quantify the phenomenon of lateral dynamic instability, mainly focusing on simple oscillators. Among the most important early achievements in the field one can distinguish Jennings and Husid [1], Al-Sulaimani and Roessett [2], Bernal [3, 4] and MacRae [5], a concise summary appearing in Miranda and Akkar [6].

The concept of dynamic instability has been recently popularized by the emergence of incremental dynamic analysis (IDA, Vamvatsikos and Cornell [7]) which nicely illustrates the termination of a system's dynamic demand/capacity curve (or IDA curve) at a maximum value of the seismic intensity (termed the *flatline*), which is unique for every ground motion record. With the advent of performance-based earthquake engineering, recent research activity has focused extensively on the prediction of the global dynamic instability and its use in loss estimation, using IDA as the main vehicle. For example, Ibarra [8] has worked extensively on the lateral collapse capacity of oscillators and simplified frames while Haselton [9] has studied in detail the collapse capacity of reinforced concrete frames. Goulet et al. [10] have used collapse capacity information to calculate building seismic losses while Liel et al. [11] and Dolsek [12] have introduced modeling uncertainties to the collapse estimation of reinforced-concrete frames. Finally, Kanvinde [13] and Lignos [14] have offered experimental verification of dynamic lateral instability in steel moment-frames.

Despite the emergence of IDA, the need for simplified methods for professional practice still remains. The rational answer has been the use of an equivalent single-degree-of-freedom (SDOF) system used as a proxy for multi-degree-of-freedom (MDOF) model behavior. Using approximate $R$-$\mu$-$T$ equations to evaluate the mean ductility $\mu$ response of the equivalent oscillator for a given period $T$ and strength ratio (or strength reduction factor) $R$ the well-known static pushover method was born [e.g., 15]. Unfortunately, such procedures are based on the positive stiffness part of the pushover curve, using $R$-$\mu$-$T$ relationships from bilinear elastoplastic oscillators that do not exhibit any lateral instability. Hence, almost all such approximations enable unreasonably large values of the strength reduction factor $R$ to be attainable. It appears as if, regardless of the system's properties and stability, it is not in danger of dynamic instability at any seismic intensity level. In that sense, there has been a need for a limiting value of $R$ for all systems that eventually exhibit negative stiffness and have the potential for global dynamic instability.

Building upon the SDOF system approximation, it was only natural to use it to assess MDOF collapse capacity [4, 16]. This leads to a system-specific limiting value on the $R$ strength ratio that, following the work of Miranda and Akkar [6], we will term the *collapse strength ratio* and symbolize as $R_c$. This quantity, among others, was precisely captured by Vamvatsikos and Cornell [17, 18] for oscillators with quadrilinear force-deformation backbones, using the complex computational tool SPO2IDA [19]. Actually, SPO2IDA is a much more general tool, aiming to reproduce more than just the limiting value of $R_c$; the scope of its application necessitated the use of complex equations encapsulated within a spreadsheet, without offering an easy-to-use, single formula. This need was identified by Miranda and Akkar [6] who introduced a sim-

plified equation for $R_c$ for bilinear, elastic-negative backbones. It was also further promoted by the FEMA440 guidelines [20] which replaced the controversial $C_3$ "P-Δ" coefficient of the FEMA356 method [15] with a limiting value on the system's strength ratio, $R_{\max}$. While this is an explicit recognition of the need for quantifying global collapse capacity, it is actually a conservative boundary-value meant to set an upper limit on the applicability of pushover-based procedures.

A final breakthrough came with the work of Vamvatsikos and Cornell [21] who showed that oscillator $R_c$ values can be used to approximate with reasonable accuracy the dynamic instability of even complex, higher-mode-sensitive structures. The basic premise is that even complicated structures tend to lose their complex behavior as more and more plastic hinges form. Thus, when the structure approaches collapse it tends to vibrate in practically a single, energy-efficient pattern, rather than several ones. If the static pushover is able to find the controlling collapse mechanism, a task that may necessitate using several different load patterns, then $R_c$ can be used to estimate global dynamic instability.

In light of the above developments, it is important to have an accurate, yet simple enough equation that can provide the statistics, e.g., a central value (mean/median) and a dispersion measure, for the $R_c$ of non-trivial oscillators. In effect, we need an equation that can bridge the gap between the conservative FEMA440, the too-simple bilinear backbone of Miranda and Akkar [6] and the rather complex quadrilinear backbone of Vamvatsikos and Cornell [18]. In the sections to follow, we aim to provide such an approach, using an oscillator having a non-trivial, trilinear backbone and arbitrary period.

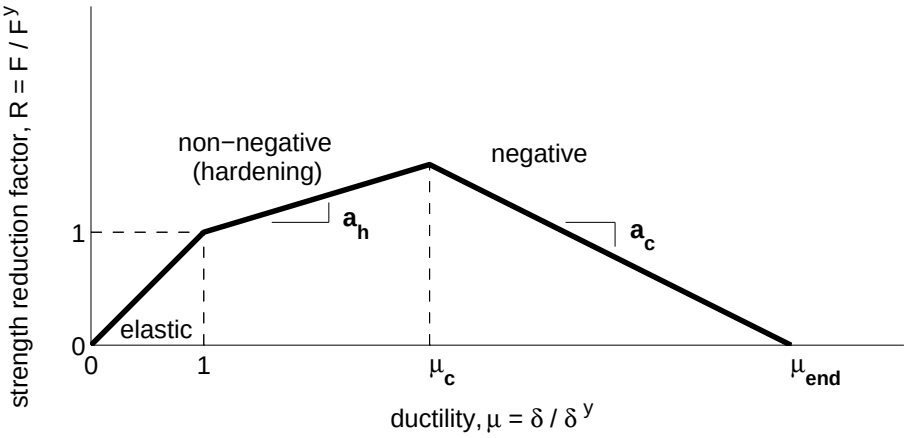


Figure 1: The backbone to be investigated and its three controlling parameters, $a_h$, $\mu_c$ and $a_c$.

## 2 OSCILLATOR BACKBONE AND HYSTERESIS

Since our aim is to capture the global dynamic instability, or collapse capacity, of oscillators and (eventually) structures, we need to refrain from the typical elastic-plastic or elastic-hardening backbones that are typically used in the literature. What we need beyond the elastic is at least (a) a plastic or hardening branch to simulate the post-yield ductility and (b) a negative stiffness branch that is typical of the behavior of most structures, either brittle or ductile, that reach a maximum strength and then exhibit in-cycle degradation that leads them to strength loss and negative stiffness. The reasons behind the negative stiffness in an actual structure maybe P-Δ effects, material strength degradation or a combination of the two. Both of these effects will be uniformly represented by the negative-stiffness slope of the force-deformation backbone.

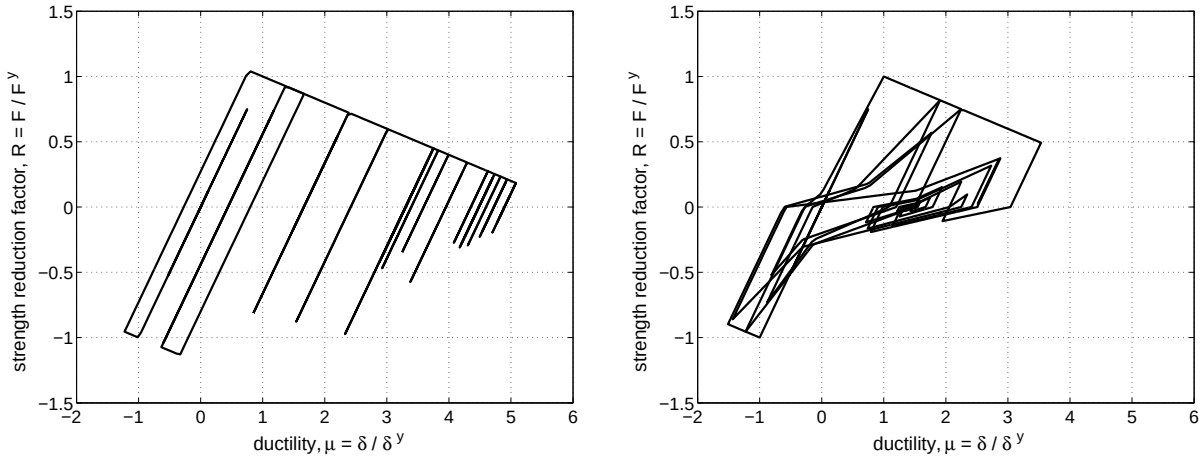


(a) Kinematic hysteresis.

(b) Pinching hysteresis.

Figure 2: The effect of hysteresis modeling on the dynamic response of an elastic-negative backbone with $a_c = -0.2$, $T = 1$s. The same record and intensity are used in both cases (from Vamvatsikos and Cornell [18]).

While the backbone described above seems to be general enough, systems like braced-frames and reinforced-concrete frames with masonry infills that exhibit a significant residual-strength segment are not adequately captured. As work in SPO2IDA has shown [18], when the segment is of significant height or significant length it cannot be ignored, although doing so is always a conservative assumption.

Hence, we have focused on a trilinear backbone featuring an elastic, a hardening (non-negative stiffness), and a negative slope segment. Figure 1 shows the shape of the backbone in normalized coordinates of the strength ratio (or reduction factor), $R = F/F^y$, versus ductility $\mu = \delta/\delta^y$, where $\delta$ is the oscillator displacement and $F$ its force, with the superscript $y$ denoting their value at yield. The backbone starts with an elastic segment that stops with the yield point at $(R,\mu) = (1,1)$, then continues at a reduced stiffness ratio of $a_h$ ($0 \le a_h < 1$) times the elastic, ending at ductility $\mu_c$ ($1 < \mu_c$), termed the capping ductility (e.g., Ibarra [8]). Finally, the backbone starts on a descending slope that is of negative stiffness $a_c$ ($a_c < 0$) times the elastic. Zero strength is reached at the ultimate ductility $\mu_{\text{end}} = \mu_c + (1 + a_h\mu_c - a_h)/|a_c|$.

For the hysteresis of the system we are faced with a difficult choice. The typical solution would have been the kinematic hardening rule of the elastic perfectly-plastic system. Unfortunately, the kinematic rule is not as stable or realistic as we may want where negative stiffness is concerned. For example, as observed at least by Rahnama and Krawinkler [22] and Vamvatsikos and Cornell [18] the ratcheting behavior of the kinematic loading-unloading leads to a severe loss of capacity that may not be realistic, while the hair-comb pattern of hysteretic loops is actually not representative of the global force-deformation behavior of actual structures, as seen in Figure 2(a). On the other hand, the hysteresis loops of a pinching model, shown in Figure 2(b), or any other similar peak-oriented model, are much more realistic and better represent what we have seen in experiments and expect from an actual structure. Since the two types of hysteresis loops provide quite different collapse capacities [e.g., 18], it makes sense to stay with the pinching model for backbones with negative stiffness.

Thus, we chose a moderately pinching model without any cyclic strength degradation, as shown in Figure 3. The degree of pinching, the small details of the hysteresis loop and the existence of strength degradation have been shown by Ibarra [8] to be of secondary importance

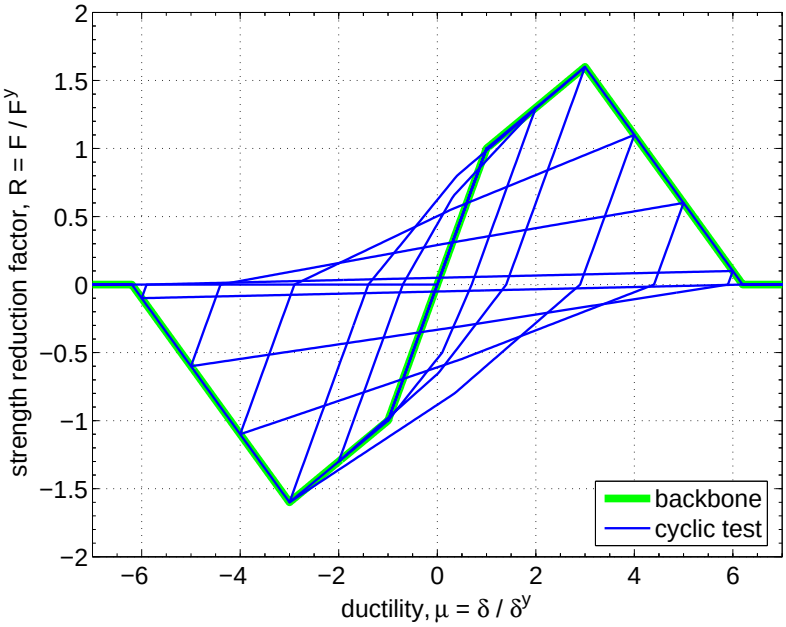


Figure 3: The backbone and hysteresis loops of a system with $a_h = 0.30$, $\mu_c = 3$ and $a_c = -0.50$.

compared to the backbone shape. Notably, the only exception is having severe strength degradation coupled with relatively short oscillator periods that lead to a system that undergoes many strength-reversal cycles within the duration of an earthquake and will collapse prematurely. Since it can be relatively difficult to establish the global cyclic degradation characteristics of MDOF systems, we chose to maintain a cycle-independent backbone.

## 3 ESTIMATION OF COLLAPSE CAPACITY

In order to estimate the collapse capacity of the SDOF systems we employ incremental dynamic analysis (IDA, Vamvatsikos and Cornell [7]). IDA involves subjecting the model to a series of nonlinear dynamic analyses under a suite of ground motion records that are suitably scaled to multiple levels of intensity. A ground motion suite of 72 records was used to assess the SDOF systems (Table 1). They were recorded in nine different earthquakes with moment magnitudes 6.0 – 7.4 and in distances ranging within 12.3 – 123.9 km from the fault rupture. All records were obtained from firm soil sites of class D according to the U.S. Building Seismic Safety Council [23, 24].

Each dynamic analysis can be characterized by the level of intensity of the ground motion record characterized by the intensity measure, and a measure of the structural response, the engineering demand parameter. Typically, as intensity measure we use the 5%-damped first-mode spectral acceleration $S_a(T,5\%)$, or, in our case, its value normalized by the $S_a$ that causes first yield: $S_a^y$. The resulting intensity measure is actually coincident with the strength ratio $R = S_a/S_a^y = F/F^y$, where $F$ is the oscillator force. For the demand parameter we can use the peak displacement $\delta$ or, even better, its normalized value, the ductility $\mu = \delta/\delta^y$, where $\delta^y$ is the displacement at yield.

Thus each dynamic analysis can be represented by a single point in the same $R$-$\mu$ plane as the oscillator's backbone. If such points for a given record are interpolated by a flexible curve, e.g., a spline (Vamvatsikos and Cornell [25]), a continuous IDA curve is created, one for every record, as seen for a suite of 72 records in Figure 4. Such curves start out elastic and either harden to higher slopes or soften to lower ones, but eventually, as the intensity increases, they

| Event | Station | M[1] | $R_e$[2] (km) | $R_n$[3] (km) | $\phi_1$ (deg) | PGA (g) | $\phi_2$ (deg) | PGA (g) |
|---|---|---|---|---|---|---|---|---|
| Borrego Mtn, 1968 | El Centro #9 | 6.8 | 45.0 | 29.5 | 180 | 0.13 | 270 | 0.06 |
| Imperial Valley, 1979 | El Centro #12 | 6.5 | 18.0 | 32.1 | 140 | 0.14 | 230 | 0.12 |
| Imperial Valley, 1979 | Plaster City, Storehouse | 6.5 | 32.0 | 54.4 | 135 | 0.06 | 045 | 0.04 |
| Imperial Valley, 1979 | Calexico, Fire Station | 6.5 | 10.6 | 17.4 | 225 | 0.27 | 315 | 0.20 |
| Imperial Valley, 1979 | El Centro #3 | 6.5 | 12.7 | 31.7 | 140 | 0.27 | 230 | 0.22 |
| Imperial Valley, 1979 | El Centro #11 | 6.5 | 12.6 | 30.1 | 140 | 0.36 | 230 | 0.38 |
| Imperial Valley, 1979 | Brawley, Municipal Airport | 6.5 | 8.5 | 46.3 | 225 | 0.17 | 315 | 0.22 |
| Imperial Valley, 1979 | Coachella, Canal #4 | 6.5 | 49.0 | 86.8 | 045 | 0.12 | 135 | 0.13 |
| Kern County, 1952 | LA, Hollywood Sto. PE Lot | 7.4 | 107.0 | 118.8 | 090 | 0.04 | 180 | 0.06 |
| Landers, 1992 | Yermo, Fire Station | 7.3 | 26.3 | 85.8 | 270 | 0.24 | 360 | 0.15 |
| Landers, 1992 | Palm Springs, Airport | 7.3 | 28.2 | 41.8 | 000 | 0.08 | 090 | 0.09 |
| Landers, 1992 | Fort Irwin | 7.3 | 65.5 | 120.9 | 000 | 0.11 | 090 | 0.12 |
| Landers, 1992 | Baker, Fire Station | 7.3 | 88.3 | 123.9 | 050 | 0.11 | 140 | 0.11 |
| Landers, 1992 | Pomona, 4th and Locust FF | 7.3 | 117.6 | 122.0 | 000 | 0.07 | 090 | 0.04 |
| Loma Prieta, 1989 | Gilroy #2 | 6.9 | 12.1 | 29.5 | 090 | 0.32 | 000 | 0.40 |
| Loma Prieta, 1989 | Gilroy #3 | 6.9 | 14.0 | 31.1 | 090 | 0.37 | 000 | 0.54 |
| Loma Prieta, 1989 | Agnews State Hospital | 6.9 | 27.0 | 40.0 | 090 | 0.16 | 000 | 0.17 |
| Loma Prieta, 1989 | Hayward, John Muir School | 6.9 | 58.9 | 71.0 | 090 | 0.14 | 000 | 0.17 |
| Loma Prieta, 1989 | Oakland, two story bldg | 6.9 | 76.3 | 91.9 | 290 | 0.24 | 200 | 0.19 |
| Loma Prieta, 1989 | Richmond, City Hall Prkg | 6.9 | 92.7 | 107.7 | 280 | 0.11 | 190 | 0.13 |
| Morgan Hill, 1984 | Gilroy #3 | 6.2 | 14.4 | 37.6 | 000 | 0.18 | 090 | 0.19 |
| Morgan Hill, 1984 | Gilroy #7 | 6.2 | 13.7 | 37.6 | 000 | 0.19 | 090 | 0.11 |
| Northridge, 1994 | LA, Hollywood Stor. Bldg | 6.7 | 24.8 | 22.9 | 360 | 0.39 | 090 | 0.23 |
| San Fernando, 1971 | LA, Hollywood Stor. Bldg | 6.6 | 23.0 | 24.0 | 090 | 0.21 | 180 | 0.17 |
| San Fernando, 1971 | Santa Ana, Enginering Bldg | 6.6 | 71.5 | 88.2 | 176 | 0.03 | 266 | 0.03 |
| San Fernando, 1971 | Vernon, Cmd Terminal | 6.6 | 33.5 | 49.2 | 187 | 0.08 | 277 | 0.11 |
| Whittier, 1987 | Bell LA Bulk Mail Center | 6.0 | 10.6 | 12.3 | 010 | 0.33 | 280 | 0.45 |
| Whittier, 1987 | Vernon, Cmd Terminal | 6.0 | 11.1 | 13.1 | 007 | 0.27 | 277 | 0.24 |
| Whittier, 1987 | Downey, Co. Maint. Bldg | 6.0 | 16.2 | 17.0 | 180 | 0.20 | 270 | 0.15 |
| Whittier, 1987 | LA, Hollywood Stor. Bldg | 6.0 | 23.8 | 25.0 | 000 | 0.21 | 090 | 0.11 |
| Whittier, 1987 | LA, Century City C.Club S | 6.0 | 29.6 | 32.0 | 000 | 0.06 | 090 | 0.07 |
| Whittier, 1987 | Pomona 4th, and Locust FF | 6.0 | 29.9 | 30.4 | 012 | 0.07 | 102 | 0.05 |
| Whittier, 1987 | Long Beach, Harbor Admin | 6.0 | 32.8 | 35.9 | 000 | 0.05 | 090 | 0.07 |
| Whittier, 1987 | Rancho Cucamonga | 6.0 | 45.5 | 47.0 | 090 | 0.06 | 360 | 0.05 |
| Whittier, 1987 | Arleta, Nordhoff Fire Sta. | 6.0 | 45.7 | 39.0 | 180 | 0.09 | 270 | 0.09 |
| Whittier, 1987 | Rosamond, Goode Ranch | 6.0 | 89.0 | 87.0 | 000 | 0.08 | 090 | 0.05 |

Note: M = moment magnitude, PGA = peak ground acceleration, $\phi_1$, $\phi_2$ = component directions, $R_e$ = epicentral distance, $R_n$ = closest distance to horizontal projection of fault rupture.

Table 1: The 72 records used, all recorded on NEHRP soil site D.

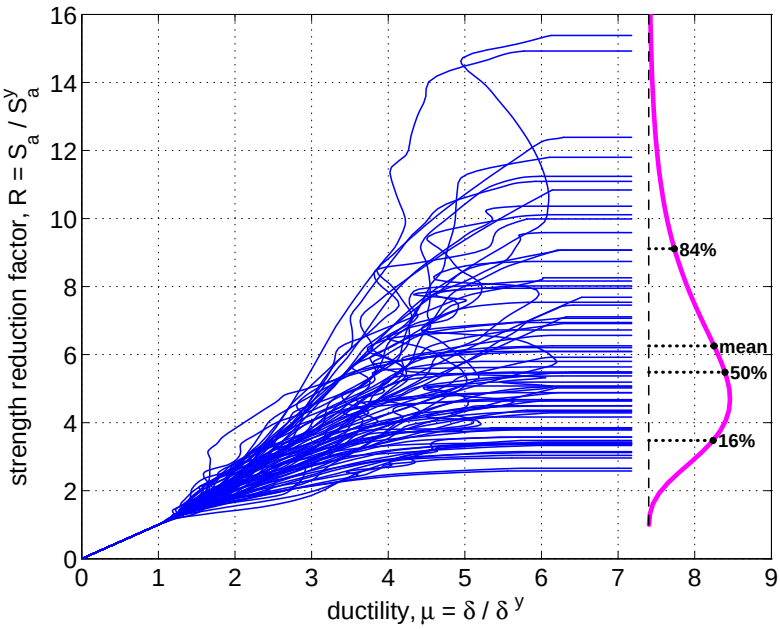


Figure 4: The 72 IDA curves and the distribution of their $R_c$ capacities for a system with $a_h = 0.30$, $\mu_c = 3$, $a_c = -0.50$ and $T = 1.0$s.

all succumb and reach a final flatline at a specific normalized intensity $R_c$, beyond which the oscillator shows infinite response $\mu$ for the given accelerogram. This value signals the onset of dynamic instability for the system and it is precisely indicative of its collapse capacity, assuming the numerical integration has been performed accurately. As it becomes obvious in Figure 4, each record has its own characteristic value of $R_c$, showing an overall wide dispersion that can only be characterized by a probabilistic distribution. As seen in Figure 4 and rigorously verified by a Kolmogorov-Smirnov test [e.g., 26] (at least at the 95% confidence level), the lognormal distribution is a good model to use for $R_c$, confirming the observations of several researchers [e.g., 18].

In order to characterize $R_c$ we need to supply appropriate summarized statistics. In similar approximate $R-\mu-T$ equations the typical estimate provided is the mean value, be it the mean $R$ or the mean $\mu$ (e.g., see [20, 27] and references therein). Unfortunately supplying just the mean is inadequate for complete characterization of $R_c$ and it is not as useful within a performance-based earthquake engineering framework, e.g., such as the one pioneered by SAC/FEMA [28] or the Pacific Earthquake Engineering Research Center (Cornell and Krawinkler [29]). In order to appropriately capture the distribution of $R_c$ we need to provide at least a central value, e.g., the mean or the median of the distribution, and a measure of dispersion, e.g., the variability or the standard deviation.

For reasons of simplicity and better description of the distribution, we chose to focus on four different statistics of $R_c$: The mean value $R_{c,m}$ and the 16%,50% (median),84% percentiles, $R_{c,16\%}$, $R_{c,50\%}$, $R_{c,84\%}$, i.e., the values below which lie 16,50 and 84% of the sample $R_c$-values respectively. The three percentiles are actually the same quantities that SPO2IDA also provides, while the mean is added for reasons of consistency with current practice. Nevertheless, it should be noted that for a perfectly lognormal variable, any two of the above would be enough to completely define it, actually needing only the mean or median and the dispersion. For example, assuming lognormality, we can use the 16, 84% values to estimate the standard deviation of the

logs,

$$\beta = \frac{\ln(R_{c,84\%}) - \ln(R_{c,16\%})}{2}. \quad (1)$$

and the average of their logs to determine the log-mean. Alternatively, since we are typically interested in the lower percentiles of capacity, i.e., those that are more likely to cause failure, it may make sense to fit locally in the lower part of the $R_c$ distribution, using the following equation:

$$\beta = \ln(R_{c,50\%}) - \ln(R_{c,16\%}) \quad (2)$$

Actually, both of the above approximations are exact for a lognormal distribution, but will never yield the exact same results for our limited sample. Nature does not necessarily conform to our models, therefore it helps to collect as much information as possible. We can use the derived fractile values to better characterize our distribution and maybe look for more refined models than just the lognormal. The principal advantage of this approach is that we can derive a wealth of information on the distribution of $R_c$ using the same approximating equation for each of the four quantities of interest. Devising and fitting such an equation is going to be our next goal.

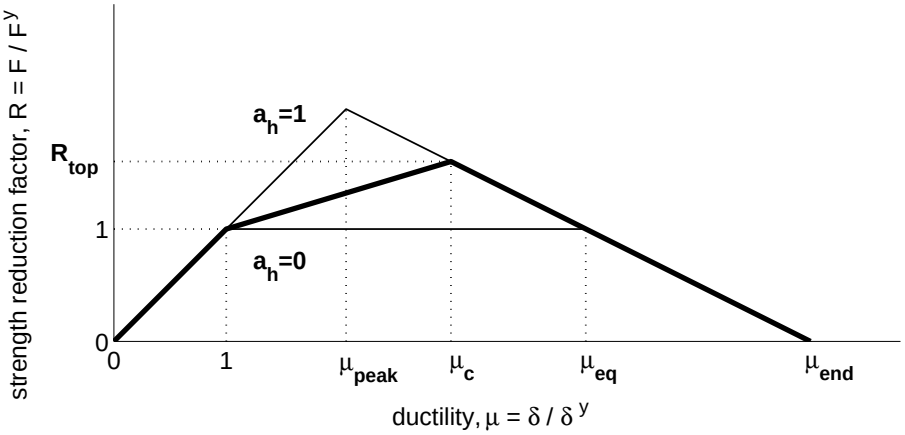


Figure 5: An elastic-hardening-negative backbone and the two extremes of its "equivalent" set.

## 4 DEVELOPING APPROXIMATE EQUATIONS

In our quest for devising simple equations for the estimation of summarized values of $R_c$ we find ourselves facing the classic problem of modeling a multi-parameter system. The trilinear backbone that we are using needs four parameter to define its shape, to which we should also add the oscillator period. In essence, we have a 4-parameter space that will be very difficult to populate with sufficient data and also fit by a relatively simple equation. Therefore, we will use simpler oscillator backbones to try and approximate the effect of the trilinear. To that effect we turn to the principles pioneered by SPO2IDA [18]. The idea is to use the elastic-negative backbone and the elastic-plastic-negative as simpler building blocks to build-up the more elaborate elastic-hardening-negative backbone.

The above ideas, complemented by extensive testing, have shown that, for a given period $T$, the summarized collapse capacities (mean or percentiles) $R_c^{hn}$ of the elastic-hardening-negative backbone with parameters $a_{h0}$, $\mu_{c0}$, $a_{c0}$ and $T_0$ can be built up from

a) $R_c^n$, the collapse capacities of the elastic-negative system with parameters $a_c = a_{c0}$ and $T = T_0$.

b) $\mu_{\text{peak}} \times R_c^n$, the collapse capacities of the elastic-negative system with parameters $a_c = a_{c0}$ and $T = T_0$ but with the yield point shifted to ductility $\mu = \mu_{\text{peak}}$, rather than $\mu = 1$ (see Figure 5), where

$$\mu_{\text{peak}} = \frac{\mu_c |a_c| + 1 + a_h(\mu_c - 1)}{1 + |a_c|}. \tag{3}$$

c) $R_c^{pn}$, the collapse capacities of the elastic-plastic-negative system with parameters $a_h = 0$, $a_c = a_{c0}$ and $\mu_c = \mu_{\text{eq}}$, where

$$\mu_{\text{eq}} = \mu_c + \frac{a_h(\mu_c - 1)}{|a_c|}. \tag{4}$$

The latter two backbones are actually the boundaries of what has been termed an "equivalent set" by Vamvatsikos and Cornell [18] which comprises all the trilinear backbones of varying $a_h \in [0,1]$ that have coincident negative-stiffness segments, as shown in Figure 5. Within an equivalent set, the mean and percentile values of $R_c$ vary linearly between the two extremes, i.e., the $a_h = 0$ and the $a_h = 1$ cases where the negative branch starts at capping ductilities $\mu_{\text{eq}}$ and $\mu_{\text{peak}}$ respectively. So we only need to model the capacities for the extreme values of $a_h$ and linearly interpolate in-between. In this way, we have effectively removed $a_h$ from the four parameters to be investigated, reducing the dimensionality of our problem by one.

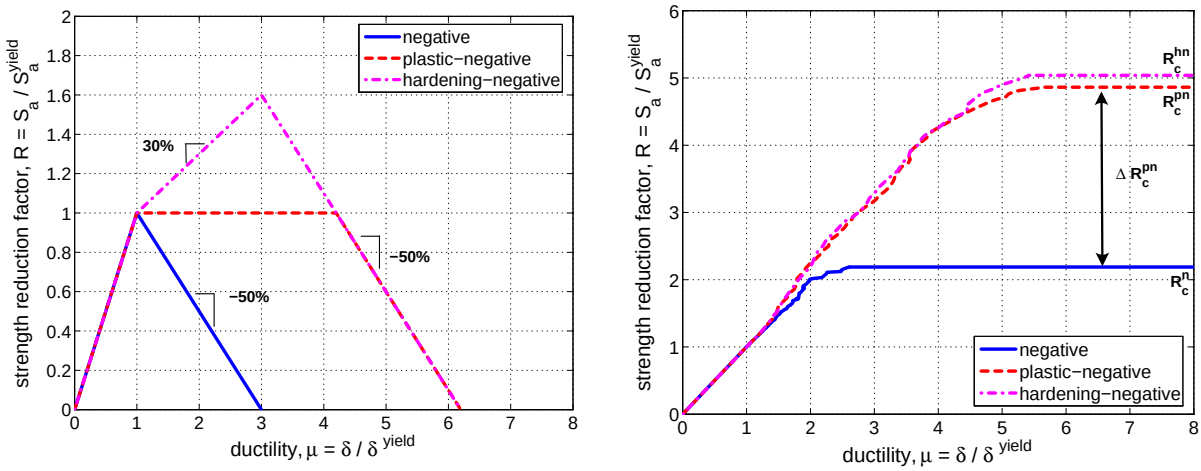


(a) The backbones used for predicting $R_c$.

(b) The corresponding median IDAs.

Figure 6: The definition of the dynamic-instability capacities, $R_c^n$,$R_c^{pn}$ and $R_c^{hn}$ for an elastic-negative, an elastic-plastic-negative and an elastic-hardening-negative system respectively, showing (a) the backbones and (b) the corresponding median IDA curves.

Hence, we only need to estimate $R_c^n$, which depends on $(a_c, T)$, and $R_c^{pn}$, which is a function of $(a_c, \mu_c, T)$. Further simplifications are possible if we model instead only $R_c^n$ and the difference of the two, $\Delta R_c^{pn} = R_c^{pn} - R_c^n$. Extensive tests have shown that, to a high degree of accuracy, we can assume $\Delta R_c^{pn}$ to be independent of $a_c$. In other words, $\Delta R_c^{pn}$ is a term that represents solely the additionally effect of the plastic plateau and depends on its length $\mu_c$ and the oscillator period $T$. In this way, we have reduced our original 4-parameter problem into two 2-parameter ones. The difference in the needed computations is vast; if we decide to use $N$ samples for each of the four parameters, then we need $N^4$ samples to accurately cover the

Table 2: The coefficients needed to calculate the mean and fractiles of the dynamic instability capacity of elastic-negative and elastic-plastic-negative backbones using Equations (5) and (6).

| | coefficient | 16% | 50% | 84% | mean |
|---|---|---|---|---|---|
| $R_c^n$ | $\beta_1$ | 0.07 | 0.35 | 1.50 | 0.37 |
| | $\beta_2$ | 1.11 | 1.32 | 1.32 | 1.29 |
| | $\beta_3$ | 0.03 | 0.19 | 0.14 | 0.12 |
| | $\beta_4$ | 0.19 | 0.29 | 0.15 | 0.16 |
| $\Delta R_c^{pn}$ | $\gamma_1$ | 0.77 | 1.20 | 1.90 | 1.20 |
| | $\gamma_2$ | 0.80 | 1.00 | 2.40 | 2.00 |
| | $\gamma_3$ | 5.50 | 2.70 | 0.50 | 1.90 |

parameter space of the original problem, while only $2N^2$ samples for the reduced one, realizing savings of two orders of magnitude. That, combined with the simplicity of devising and fitting 2-parameter rather than 4-parameter equations proves the value of our approach.

The proposed breakdown of the problem is explained graphically in Figure 6. Figure 6(a) shows an elastic-hardening-negative backbone and the two backbones that will be used to estimate its collapse capacity. Figure 6(b) shows the definition of the median $R_c^n$ and $R_c^{pn}$ strength ratios, their difference $\Delta R_c^{pn}$, and the additional (albeit small in this case) effect of the hardening slope $a_h$ that distinguishes the final capacity $R_c^{hn}$ from $R_c^{pn}$. The effect is similar for the mean or the other percentile values.

For each of the $R_c^n$ and $\Delta R_c^{pn}$ terms we tested several functional forms and came up with simple three and four parameter approximations, respectively. For the pure pinching elastic-negative backbone, we used

$$R_c^n(a_c,T) = 1 + \left(1.17 - \mathrm{e}^{-\beta_1 T}\right) |a_c|^{-\beta_2+\beta_3 T-\beta_4 \ln T}, \tag{5}$$

while for the additional influence of the plastic plateau we chose

$$\Delta R_c^{pn}(\mu_c,T) = \gamma_1 (\mu_c - 1) \left[1 - \mathrm{e}^{\left(-\gamma_2 (\gamma_3)^{\frac{1}{\mu_c}} T\right)}\right]. \tag{6}$$

In order to determine the parameters for the mean and percentile values we performed two-stage nonlinear regressions for $a_c \in [-4,-0.01]$, $\mu_c \in [1,9]$ and $T \in [0.2,3]$s. The best-fit values appear in Table 2 and allow the estimation of any of the four quantities of interest (mean and 16,50,84% percentiles). Representative plots showing the behavior of the median $R_c^n$ and $\Delta R_c^{pn}$ according to Equations (5),(6) appear in Figures 7(a) and 7(c), while the corresponding $\beta$-dispersion values, as determined according to Equation (1), appear in Figures 7(b) and 7(d).

Predictably, the median (and correspondingly the mean and any other percentile) of $R_c^n$ rapidly drops with steeper negative slopes $a_h$ and lower periods $T$. Its dispersion is similarly reduced for lower periods and for the higher negative slopes (in absolute terms). This makes sense as both short periods and steep slopes tend to hasten the arrival of dynamic instability in $R$-terms, squeezing all records together to similar values of $R_c$ as $a_c$ approaches minus infinity. For example, a perfectly brittle system whose backbone drops to zero right after yielding has $R_c = 1$ regardless of the ground-motion record used, resulting to zero dispersion. This is actually the major effect that we are seeing in Figure 7(b).

On the other hand, the median $\Delta R_c^{pn}$ is relatively less dramatic in its behavior, rising almost linearly with $\mu_c$ for all but the lowest values of $T$. In the short period range or for the lowest

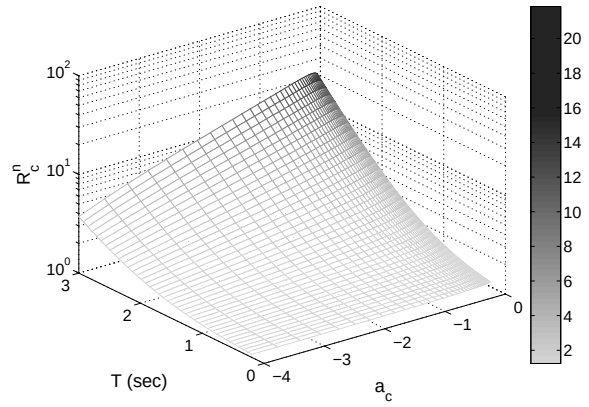


(a) The median value of $R_c^n$ versus $a_c$ and $T$.

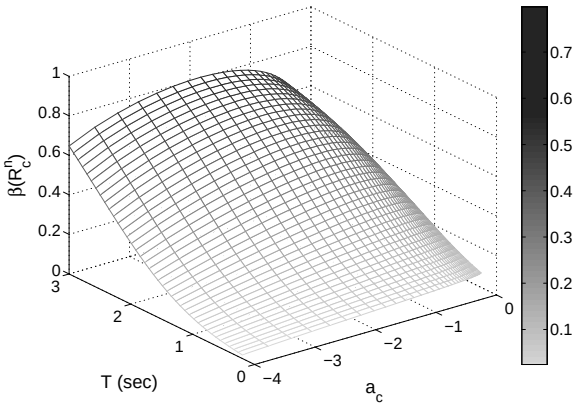


(b) The dispersion of $R_c^n$ versus $a_c$ and $T$.

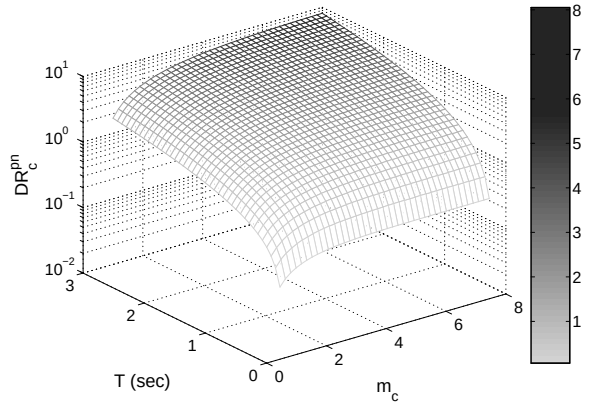


(c) The median value of $\Delta R_c^{pn}$ versus $\mu_c$ and $T$.

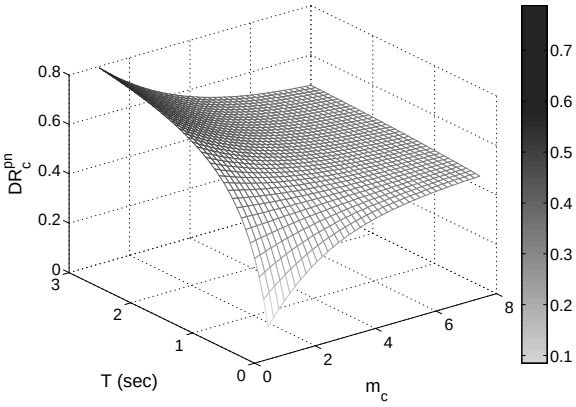


(d) The dispersion of $\Delta R_c^{pn}$ versus $\mu_c$ and $T$.

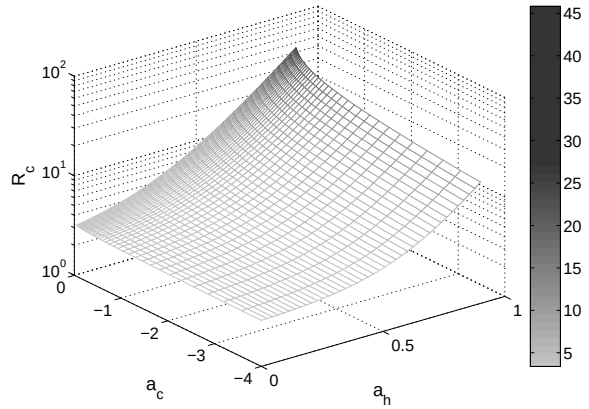


(e) Median $R_c$ versus $a_h$, $a_c$ for $\mu_c = 3$ and $T = 1$.

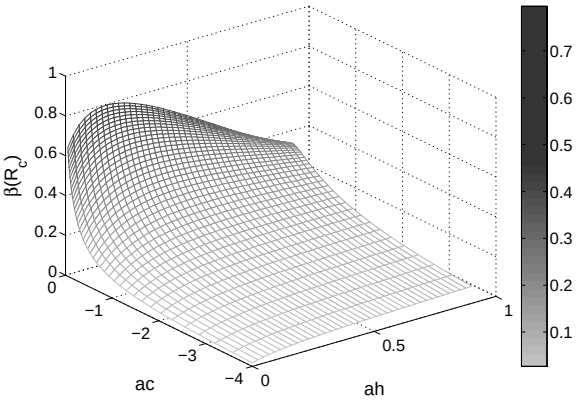


(f) Dispersion of $R_c$ versus $a_h$, $a_c$ for $\mu_c = 3$ and $T = 1$.

Figure 7: The median and beta of the $R$-capacities predicted by Equations (5), (6) and (8).

$\mu_c$'s close to 1 we see a definite change in slope, signaling decreased gains from the plastic plateau: Unless the plateau is of some reasonable length $\mu_c > 1.5$ and we are away from the low period range, it will not be of significant help. The dispersion shown in Figure 7(d) presents again a near-zero value for low periods and low $\mu_c$'s for the same reason described before: The $R_c$'s of individual records are being squeezed to unity, thus there is little room for dispersion. Interestingly, the dispersion is almost independant of $T$ for $\mu_c$ >2, while it becomes quite large for low $\mu_c$ and longer periods. The reason seems to be that the short length of the plastic plateau combined with the longer periods has a record-dependent effect. Some records are affected by it and increase their $R_c$ value, while others are not.

Now, having Equations (5),(6) at our disposal, we can easily calculate the total capacity for any elastic-plastic-negative backbone as

$$R_c^{pn}(a_c,\mu_c,T) = R_c^{n}(a_c,T) + \Delta R_c^{pn}(\mu_c,T) \tag{7}$$

Finally, the total capacity for the elastic-hardening-negative system, which was denoted as $R_c^{hn}$ but will be simply referred to as $R_c$, can be calculated easily using the equivalent set concept (Figure 5). All we have to do is substitute $\mu_{\text{eq}}$ for $\mu_c$ in Equations (6) and (7) and use $a_h$ to interpolate between $\mu_{\text{peak}} \times R_c^n$ and $R_c^{pn}$:

$$\begin{aligned} R_c = R_c^{hn}(a_h,a_c,\mu_c,T) &= R_c^{pn}(a_c,\mu_{\text{eq}},T) + a_h\left[R_c^{pn}(a_c,\mu_{\text{eq}},T) - \mu_{\text{peak}}R_c^{n}(a_c,T)\right] \\ &= \left[1 - a_h\left(\mu_{\text{peak}}-1\right)\right]R_c^{n}(a_c,T) + (a_h+1)\,\Delta R_c^{pn}(\mu_{\text{eq}},T). \end{aligned} \tag{8}$$

Sporting 4 parameters, the nature of Equation (8) is too complex to explain in a single graph. Still, it suffices to know that it inherits its properties from $\Delta R_c^{pn}$ and $R_c^n$ regarding $a_c$, $\mu_c$ and $T$. Thus, our previous observations are still valid and we only need to show its behavior versus $a_h$ to complete the circle. This final piece of information is revealed in Figure 7(e) for the given values of $\mu_c = 3$ and $T = 1$. Therein we can see that both higher values of $a_h$ and milder negative slopes $a_c$ are beneficial for the system's capacity, confirming our engineering intuition. Figure 7(f) contains the system's dispersions, showing again that steep $a_c$'s force a near-zero dispersion across the board, while low values of $a_h$ cause increased dispersion compared to higher $a_h$, confirming, in some sense, the observations of Macrae and Kawashima [30] that the elastic-plastic system is less stable than the elastic-hardening. This can be also understood if we realize that when $a_h$ is closing to unity, the hardening part starts to turn into an almost-elastic one. This should consequently have a near-zero dispersion. Therefore, we should expect to see some reduction in $\beta$ with increasing values of the hardening slope $a_h$.

## 5 ILLUSTRATIVE RESULTS

In order to showcase the power of the proposed equations, we will run a test against the best-known existing approximations for elastic-hardening-negative trilinear backbones and compare them versus the actual results from the 72 records from Table 1. The approximations tested will be (a) the SPO2IDA tool [18], (b) our own Equation (8) and (c) the FEMA440 [20] $R_{\max}$, which according to our terminology can be written as

$$R_{\max} = \mu_c + \frac{1}{4}\left|a_c\right|^{-(1+0.15\ln T)}. \tag{9}$$

While it may be reasoned that we our using the same dataset for testing that we have also used for fitting Equations (5),(6), it should be noted that we never really fit the final Equation (8)

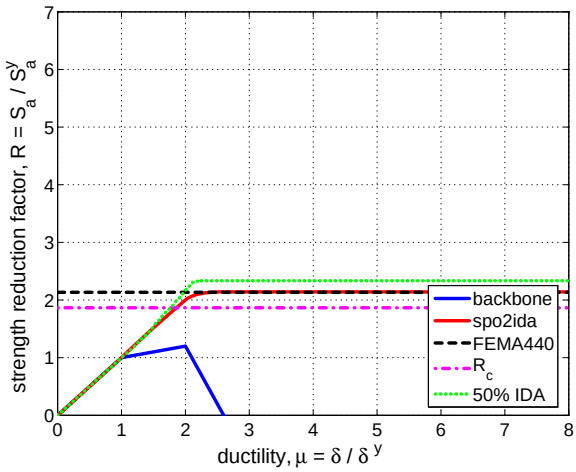


(a) non-ductile, $T = 0.5$s

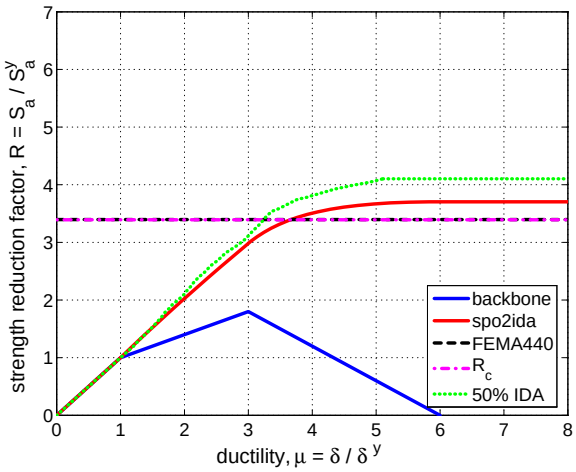


(b) ductile, $T = 0.5$s

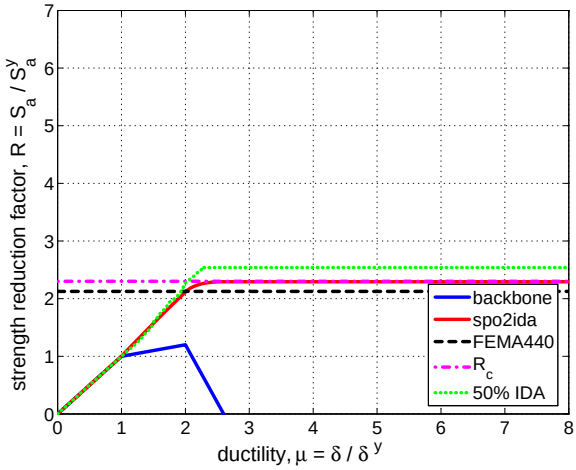


(c) non-ductile, $T = 1.0$s

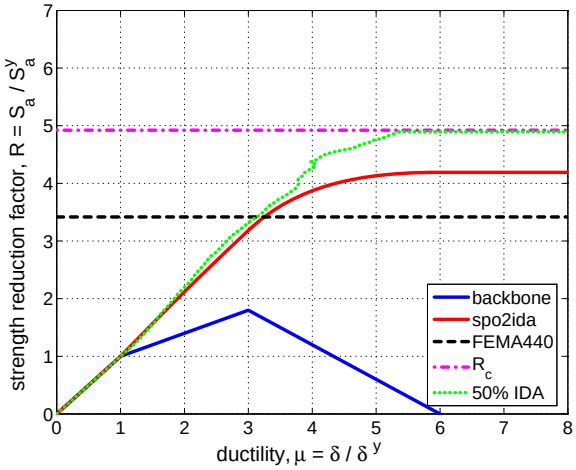


(d) ductile, $T = 1.0$s

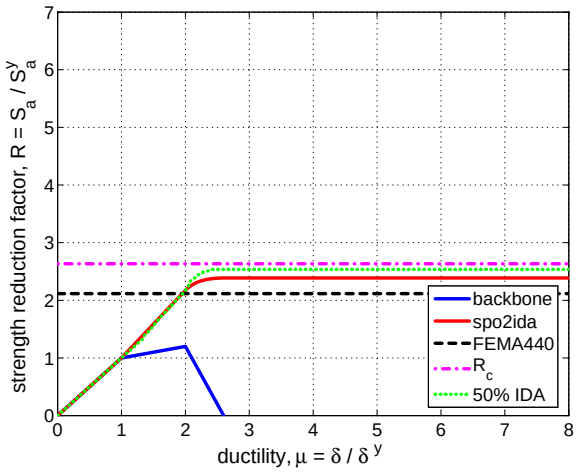


(e) non-ductile, $T = 2.0$s

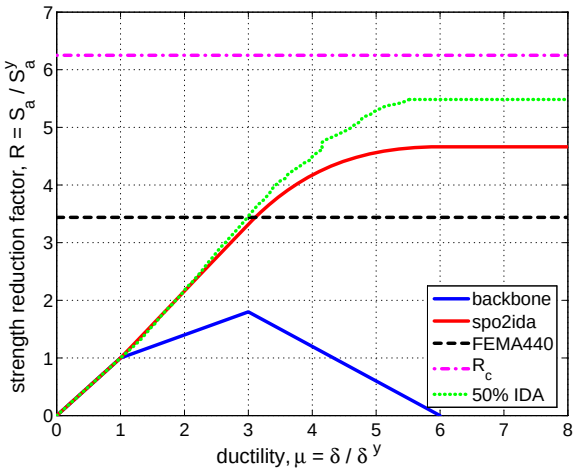


(f) ductile, $T = 2.0$s

Figure 8: The predicted $R_c$ according to FEMA440, SPO2IDA and the proposed equations for a ductile and a non-ductile system with periods $T = 0.5, 1.0, 2.0$s.

to the data. We have only fitted smaller parts of it, using carefully-selected subspaces of the actual 4-dimensional space that we wanted to approximate. As long as we stay away from elastic-negative or elastic-plastic-negative backbones we will be comparing against cases that were only fit by proxy and not directly. Furthermore, a suite of 72 ordinary records is indeed a comprehensive set for reliable testing without significant bias. Therefore, we can claim that, within reasonable bounds, we will be able to conduct a fair test using the same 72 records.

From the array of cases that we have analyzed to ascertain the accuracy of the proposed equation, we chose two representative backbones to assess each of the candidate approximations tested. One is the relatively brittle system with $a_h = 0.2$, $\mu_c = 2$ and $a_c = -2.0$ shown in the left of Figure 8 and the other is a ductile system with $a_h = 0.4$, $\mu_c = 3$ and $a_c = -0.6$, appearing in the right. Both backbones were tested for $T \in \{0.5, 1, 2\}$s to investigate low, moderate and long periods. While we are only showing and discussing median values of $R_c$, it should be understood that similar trends appear for the mean and the 16,84% values, at least regarding SPO2IDA and Equation (8) that can actually provide estimates for them.

As a first conclusion, it is obvious that across any period the ductile system always performs better than the brittle one, reaching almost double the median values of the brittle's $R_c$. Furthermore, for the same backbone, increasing periods always lead to increased $R_c$'s, a trend that both SPO2IDA and Equation (8) obviously follow but the FEMA440 $R_{\max}$ value cannot represent. Actually $R_{\max}$ is slightly decreasing with period, as seen from its definition in Equation (9). It is also hampered by the lack of an explicit treatment of the effect of $a_h$. In terms of Figure 6(b) it misses part of the increase achieved between $R_c^{hn}$ and $R_c^{pn}$ due to the effect of the hardening part. In addition, since it uses $\mu_c$ rather than the higher $\mu_{\text{eq}}$, it immediately accepts another not-so-obvious source of underestimation. Thus, the FEMA440 approximation may be quite close to the actual $R_c$ for $T = 0.5$s but then it underestimates the true value for higher periods or higher values of $a_h$ with the discrepancy increasing with $T$ and $a_h$. Therefore $R_{\max}$ is consistently lower than all other predictions. Nevertheless, $R_{\max}$ is supposed to be a conservative upper limit to warn users when entering possible dynamic instability. In that sense, it has to be said that $R_{\max}$ does indeed serve its intended purpose, but it is just adequate; it does not provide a consistent level of confidence (or safety) across all periods neither is it fit for $R_c$ prediction per se.

As expected, SPO2IDA and Equation (8) offer a more competitive estimation for all cases studied. Actually, they both have a similar error on average, in the order of 10-20%, which comes off as a small surprise. We should keep in mind here that, although based on a similar fitting concept, these two methods have important differences: SPO2IDA suffers from using a much smaller set of ground motions (30 versus 72) while Equation (8) is hampered by restricting itself to a simpler, more user-friendly equation. The comparison initially looks like a draw. Still, in the present example, SPO2IDA seems to show a consistent underestimation, albeit a low one. This bias has been observed for several other cases as well and it is a direct problem of using the smaller record sample. Had we tried this comparison versus the actual IDA results of the 30 records used to fit SPO2IDA, it would probably be Equation (8) that would show a consistent overestimating bias. Regardless, we had better trust the results of the larger sample that clearly favor the proposed equation.

Nevertheless, SPO2IDA has a distinct advantage in that it provides a full range estimation of the median (and 16%, 84%) IDA curve for all values of ductility. On the other hand, Equation (8) provides only the flatline capacity but without any bias. Therefore, each has its advantages and disadvantages and its own range of possible applications. It suffices to say, though, that any of the two, and especially Equation (8) is a vast improvement over the FEMA440 $R_{\max}$

as it can offer a much better upper limit for the use of static pushover methods. Furthermore, it is a limit that can be calibrated to deliver the desired probability of non-exceedance, in an appropriate and consistent way that is suitable for code use.

## 6 CONCLUSIONS

A new equation has been presented that can approximate the collapse capacity strength ratio of trilinear oscillators with an elastic, a hardening and a negative segment. Offering not just a central value but the median, the mean and the 16, 84% fractile values, it presents a complete characterization of the distribution of the strength ratio that will cause dynamic instability and subsequent collapse. Given the recent focus on the prediction of lateral instability, it represents a valuable tool that can find its place in codified documents and reliably replace the existing approximations, as for example in FEMA440. Furthermore, it allows for detailed, easy-to-perform parametric investigations of the effect of the backbone characteristics on its collapse capacity that is unsurpassed in providing useful understanding of the actual system's behavior. Using it, one is able to comprehend the detrimental effect of the negative slope on the structural capacity, the low significance of the hardening slope and measure the important benefits realized by longer, ductile plateaus. All in all, it is a useful tool that can easily earn a place in everyday engineering work.

## 7 ACKNOWLEDGEMENTS

The first author wishes to acknowledge the kind support of the Institute for International Education (IIE/West Coast). We also wish to thank Doctor L. Ibarra and Professor H. Krawinkler for providing the SDOF analysis program.

## References

[1] P.C. Jennings, R. Husid, Collapse of yielding structures during earthquakes. *ASCE Journal of the Engineering Mechanics Division*, **94**(5), 1045Ű1065, 1968.

[2] G.J. Al-Sulaimani, J.M. Roessett, Design spectra for degrading systems. *ASCE Journal of Structural Engineering*, **111**(12), 2611–2622, 1985.

[3] D. Bernal, Amplification factors for inelastic dynamic p-delta effects in earthquake analysis. *Earthquake Engineering and Structural Dynamics*, **15**(5), 635–651, 1997.

[4] D. Bernal, Instability of buildings subjected to earthquakes. *Earthquake Engineering and Structural Dynamics*, **118**(8), 2239–2260, 1992.

[5] G.A. MacRae, P-delta effects on single-degree-of-freedom structures in earthquakes. *Earthquake Spectra*, **10**(3), 539–568, 1994.

[6] E. Miranda, S. Akkar, Dynamic instability of simple structural systems. *ASCE Journal of Structural Engineering*, **129**(12), 1722–1726, 2003.

[7] D. Vamvatsikos, C.A. Cornell, Incremental dynamic analysis. *Earthquake Engineering and Structural Dynamics*, **31**(3), 491–514, 2002.

[8] L.F. Ibarra, Global collapse of frame structures under seismic excitations. PhD Dissertation, Department of Civil and Environmental Engineering, Stanford University, Stanford, CA, 2003.

[9] C.B. Haselton, Assessing seismic collapse safety of modern reinforced concrete frame buildings. PhD Dissertation, Department of Civil and Environmental Engineering, Stanford University, Stanford, CA, 2006.

[10] C.A. Goulet, C.B. Haselton, J. Mitrani-Reiser, et al., Evaluation of the seismic performance of a code-conforming reinforced-concrete frame building—from seismic hazard to collapse safety and economic losses. *Earthquake Engineering and Structural Dynamics*, **36**(13), 1973–1997, 2007.

[11] A.B. Liel, C.B. Haselton, G.G. Deierlein, J.W. Baker, Incorporating modeling uncertainties in the assessment of seismic collapse risk of buildings. *Structural Safety*, **31**(2), 197–211, 2009.

[12] M. Dolsek, Incremental dynamic analysis with consideration of modelling uncertainties. *Earthquake Engineering and Structural Dynamics*, 2009, in press.

[13] A.M. Kanvinde, Methods to evaluate the dynamic stability of structures Ű shake table tests and nonlinear dynamic analyses. *EERI Graduate Student Paper Competition Winner*, 2002.

[14] D.G. Lignos, Sidesway collapse of deteriorating structural systems under seismic excitations. PhD Dissertation, Department of Civil and Environmental Engineering, Stanford University, Stanford, CA, 2008.

[15] ASCE, Prestandard and commentary for the seismic rehabilitation of buildings. *Report No. FEMA-356*, prepared for the Federal Emergency Management Agency, Washington, DC, 2000.

[16] D. Bernal, Instability of buildings during seismic response. *Engineering Structures*, **20**(4-6), 496–502, 1998.

[17] D. Vamvatsikos, C.A. Cornell, Seismic performance, capacity and reliability of structures as seen through incremental dynamic analysis. *Report No. RMS-46*, RMS Program, Stanford University, Stanford, CA, 2002.

[18] D. Vamvatsikos, C.A. Cornell, Direct estimation of the seismic demand and capacity of oscillators with multi-linear static pushovers through incremental dynamic analysis. *Earthquake Engineering and Structural Dynamics*, **35**(9), 1097–1117, 2006.

[19] D. Vamvatsikos, SPO2IDA software for short, moderate and long periods, 2002, URL `http://blume.stanford.edu/pdffiles/Tech%20Reports/TR151_spo2ida-allt.xls`, [Jan 2007].

[20] ATC, Improvement of nonlinear static seismic analysis procedures. *Report No. FEMA-440*, prepared for the Federal Emergency Management Agency, Washington, DC, 2005.

[21] D. Vamvatsikos, C.A. Cornell, Direct estimation of the seismic demand and capacity of MDOF systems through incremental dynamic analysis of an SDOF approximation. *ASCE Journal of Structural Engineering*, **131**(4), 589–599, 2005.

[22] M. Rahnama, H. Krawinkler, Effects of soft soils and hysteresis model on seismic demands. *Report No. 108*, The John A.Blume Earthquake Engineering Center, Stanford University, Stanford, CA, 1993.

[23] BSSC, NEHRP guidelines for the seismic rehabilitation of buildings. *Report No. FEMA-273 (Guidelines) and FEMA-274 (Commentary)*, Building Seismic Safety Council, Washington, DC, 1997.

[24] BSSC, NEHRP recommended provisions for seismic regulations for new buildings and other structures, 2000 edition. *Report No. FEMA-368 (Provisions) and FEMA-369 (Commentary)*, Building Seismic Safety Council, Washington, DC, 2001.

[25] D. Vamvatsikos, C.A. Cornell, Applied incremental dynamic analysis. *Earthquake Spectra*, **20**(2), 523–553, 2004.

[26] J.R. Benjamin, C.A. Cornell, *Probability, Statistics, and Decision for Civil Engineers*. McGraw-Hill, New York, 1970.

[27] E. Miranda, Estimation of inelastic deformation demands of SDOF systems. *ASCE Journal of Structural Engineering*, **127**(9), 1005–1012, 2001.

[28] SAC/FEMA, Recommended seismic design criteria for new steel moment-frame buildings. *Report No. FEMA-350*, SAC Joint Venture, Federal Emergency Management Agency, Washington, DC, 2000.

[29] C.A. Cornell, H. Krawinkler, Progress and challenges in seismic performance assessment. *PEER Center News*, **3**(2), 2000, URL `http://peer.berkeley.edu/news/2000spring/index.html`, (accessed: June 18th, 2002).

[30] G.A. Macrae, K. Kawashima, Post-earthquake residual displacements of bilinear oscillators. *Earthquake Engineering and Structural Dynamics*, **26**(7), 701–716, 1997.